



Effect of light-active nanomaterials on the behavior of cadmium(II) in the presence of humic acid: the case of titanium dioxide

Peifang Wang^{a,b}, Ning Qi^{a,b}, Yanhui Ao^{a,b,*}, Chao Wang^{a,b}, Zhiyuan Wang^{a,b}

^aKey Laboratory of Integrated Regulation and Resources Development on Shallow Lakes, Ministry of Education, Hohai University, Nanjing 210098, P.R. China, Tel. +86 25 83786696; emails: pfwang2005@hhu.edu.cn (P. Wang), nicholasning1121@sina.com (N. Qi), Tel. +86 025 83787330; Fax: +86 025 83787330; emails: andyao@hhu.edu.cn (Y. Ao), cwang@hhu.edu.cn (C. Wang), zhiyuan.wang1988@hotmail.com (Z. Wang)

^bCollege of Environment, Hohai University, No. 1 Xikang Road, Nanjing 210098, P.R. China

Received 2 April 2015; Accepted 17 December 2015

ABSTRACT

The influence of photoactive nano-TiO₂ on metal behavior in the presence of humic acid (HA) in aqueous system was investigated. Our study showed that the attachment of HA onto nano-TiO₂ enhanced the adsorption ability for Cd(II). The functional groups of HA could then coordinate with Cd(II), thus enhanced Cd(II) adsorption. We found that Cd(II) adsorption by HA-TiO₂ followed pseudo-second-order kinetics. The FTIR spectra confirmed that Cd(II) adsorption was mainly ascribed to the presence of hydroxyl groups and polysaccharides/polysaccharide-like substances. The hydrogen-binding mechanism therefore accounted for the observations relating to the combination of HA and nano-TiO₂ in our study. Solar light irradiation was found to weaken Cd(II) adsorption because of the photoactive properties of titania. The photoactive TiO₂ in the aqueous system induced the degradation of the adsorbed HA, thus decreased the functional groups for the complexation of Cd(II). The results illustrated that the presence of photoactive nanomaterials (such as TiO₂) would change the bioavailability of heavy metals in aquatic environments under solar irradiation.

Keywords: Cadmium; Humic acid; Nanomaterials; Solar irradiation; Titanium dioxide

1. Introduction

The discharge of heavy-metal pollutants into the aqueous system has caused widespread concern. Heavy metals are considered to be a risk to both humans and the ecosystem because of their toxicity [1,2]. These metals can also be adsorbed by lower organisms, thus affecting the entire food chain [3]. The aqueous system suffers from the severity of such pollution depending on the spatial variation of

contamination [4]. When metals are discharged into the water, some of them exist in solution, while others accumulate in the sediments [5]. The heavy metals in sediment can be released back into the water via resuspension when the chemical conditions change [6], which leads to secondary pollution. Therefore, the mobility and distribution of heavy metals are dependent on the sediment composition and structure [7,8]. In recent years, many studies focused on heavy-metal pollution and mobility in soil, suspended particulate matter, and sediment in aqueous systems [9,10].

*Corresponding author.

Cadmium (Cd(II)) is one of the most important metal ions in nature [11]. However, it has been classified as a probable human carcinogen by US Environmental Protection Agency. The presence of Cd(II) in drinking water can induce severe health risks to humans.

The humic substances (HSs) are major components of the natural organic matter (NOM) in surface water. HSs are heterogeneous mixtures of polydispersed materials with relatively stable and complex properties [12]. The HSs are rich in oxygen-containing functionalities such as carboxylic, phenolic, hydroxylic, and quinoid groups. Humic acid (HA) accounts for a significant fraction of the HSs in nature. The detailed molecular structure of HA is difficult to define because of the complexity of its source and changes in the structure upon environmental exposure. However, several common structural features can be found within these compounds. The structural core of HA consists of aromatic and heterocyclic rings and polycyclic compounds, which are connected by carbon chains or bridges and form a loose “net” structure [13]. The core also possesses common functional groups such as carboxylic groups and phenyl groups, which play a role in complexing heavy-metal ions [14,15]. HA can also act as organic coating materials onto oxide mineral surfaces via ligand exchange. Indeed, coating of HA onto oxide mineral surfaces would significantly change their surface charge and colloidal stability, thus influences the mobility and bioavailability of oxide minerals. Many reports reported the influence of HA on the behavior of heavy metals in natural environment. El-Eswed and Khalili [16] found that HA could serve as an effective adsorbent to remove Cu(II) and Ni(II) from acidic effluents. It has also been found that HA could enhance the adsorption rate and amount of Cu^{2+} in soil minerals [17]. Furthermore, Cr(VI) could be reduced to Cr(III) with lower toxicity by HA in water and soils [18].

In recent years, it is reported that manufactured nanomaterials would inevitably enter into the environment because of their wide application in many fields. Therefore, the influence of manufactured nanomaterials on natural environment has attracted a great deal of attention. [19,20]. The presence of nanomaterials in the environment may affect the mobilization of pollutants such as organic compounds and metals because of their special properties such as high specific surface areas [21–24], crystalline structures, and great reactivities [25]. Nanotitania (nano-TiO₂) is one of the most widely used nanomaterials that has been applied in numerous industries, including cosmetics, sunscreens, paints, coatings, and photocatalysts [26]. Therefore, the discharge of titania nanoparticles into water is possible through a variety of means. TiO₂ would

induce significant effects to the environment since that it is well known that titania can absorb UV light and produce reactive radicals [27]. This point is of significance as the sun injects approximately 0.2–0.3 mol photons $\text{m}^{-2} \text{h}^{-1}$ in 300–400 nm wavelength range, with a typical UV flux near the surface of the earth being 20–30 Wm^{-2} . Therefore, the abundant solar light could induce the formation of highly reactive radicals, which could in turn influence the transformation of pollutants (such as metals and organic pollutants) in aqueous systems [28,29]. Considering these factors, it is clear that photoactive nanomaterials have a significant impact on the behavior of pollutants in the environment.

To present, a number of studies have investigated the effect of HA on the environmental behavior of heavy metals [30–32]. However, few studies discuss the effect of nanomaterials (specifically, photoactive nanomaterials) on the environmental behavior of heavy metals. The purpose of this study is to explore the influence of photoactive nano-TiO₂ on the environmental behavior of metals in aqueous systems. We investigated the adsorption of Cd(II) by nano-TiO₂ in the presence of HA, and investigated the effect of solar light irradiation on the adsorption of Cd(II). Different kinds of dynamic adsorption kinetic models of Cd(II) on HA-TiO₂ were also discussed.

2. Experimental

2.1. Materials

Nano-TiO₂ with >99.5% purity was supplied by Degussa P25 (Evonik Degussa GmbH, Düsseldorf, Germany) and was used for all experiments. Degussa P25 nano-TiO₂ has a reasonably well-defined composition of typically 80:20 anatase: rutile, which is non-porous, and has a BET surface area of $55 \pm 15 \text{ m}^2 \text{ g}^{-1}$. The average particle size of nano-TiO₂ is approximately 20 nm. HA was obtained from Sigma–Aldrich as a black crystalline powder, and was selected as a model NOM molecule that could be easily dissolved in the aqueous phase. The total organic carbon (TOC) values in the experimental process were determined using a TOC tester (Liqui TOC II, Elementar, Germany). The samples were filtered through 0.45- μm cellulose membranes before analysis (Xingya Purification Materials Co., Shanghai, China). The Cd(II) solution was prepared from $\text{Cd}(\text{NO}_3)_2 \cdot 4\text{H}_2\text{O}$ (AR, Shanghai, China). The water used for the preparation of this solution was Milli-Q[®] element ultrapure water (Integral 15). The glassware was immersed in 5% HNO₃ solution for 24 h, then washed with Milli-Q[®] water thoroughly, and dried at 333 K before use.

2.2. Attachment of HA to TiO₂ nanoparticles

The attachment experiments were conducted according to the procedure of Chen [33] with minor modifications. TiO₂ (40 mg) was added to an HA solution (200 mL, 60 mg L⁻¹) in a beaker, and stirred (by means of a magnetic stirrer) at 400 rpm. The pH was maintained at approximately 13. The resulting mixture was stirred for 9.5 h (from 7:30 to 17:00) under outdoor solar irradiation during daylight hours in May 7th–May 26th (Nanjing in China, the north latitude is 31°14′–32°37′ and the east longitude is 118°22′–119°14′) to ensure that attachment was complete. In order to acquire stable solar irradiation, the experiment was carried out outdoors (the letter G was used for representing the process was under solar irradiation). After the reaction had gone to completion, the suspension was centrifuged at 12,000 rpm for 30 min, and the precipitated solid material (HA-TiO₂) was freeze-dried and ground for use in further experiments. Attachment experiments without solar irradiation were performed indoors simultaneously using an aluminum foil to avoid light penetration (the letter A was used for representing the process was in the absence of solar irradiation). The supernatants were measured using TOC analysis and UV–vis absorption spectroscopy (UV–vis). HA-TiO₂ was characterized by Fourier transform infrared spectroscopy (FTIR, FT-IR 5700, Nicolet, USA) to investigate the functional groups present on the surfaces. Samples were prepared for FTIR by mixing freeze-dried HA-TiO₂ (2 mg) with KBr pellets (100 mg) using a pestle and mortar, and the resulting mixture was analyzed. The FTIR spectra were recorded from 400 to 4,000 cm⁻¹ at a resolution of 4 cm⁻¹ to ensure good signal-to-noise ratios.

2.3. Cd(II) adsorption experiments

Experiments for Cd(II) adsorption by HA-TiO₂ were carried out in beakers by magnetic stirring at 400 rpm. In a typical experiment, the background solution contained HA-TiO₂ (10 mg L⁻¹) and Cd(II) (40 μg L⁻¹) was treated with solar irradiation at pH 8. Cd(II) adsorption experiments were also carried out indoors simultaneously for comparison. To detect the concentration of Cd(II) in the solution, 10-mL samples were collected at 0, 5, 15, 30, 60, 90, 120, 180, and 240 min. The samples were centrifuged at a speed of 12,000 rpm for 30 min, the supernatant solutions were pipetted from the centrifuge tubes, and filtered through a 0.45-μm cellulose acetate membrane. Then the sample was acidified with HNO₃ for further analysis. The precipitated solid

materials were freeze-dried, and ground for further analysis. The dark adsorption experiments of Cd(II) were performed the same way as described above, but in the absence of solar irradiation. In summary, we used letters AA to represent the experiments carried out in the absence of solar irradiation for both processes (attachment of HA on TiO₂, Cd(II) adsorption). The letters GG to represent the experiments carried out under solar irradiation for both processes. The letters AG to represent that the Cd(II) adsorption was carried out under solar irradiation, while the attachment experiment was carried out in the absence of solar irradiation. The concentration of Cd(II) in the supernatants was measured by inductively coupled plasma mass spectrometry (ICP-MS, Agilent 7700). The experiments were performed in triplicate, and statistically similar results were obtained each time. The SPSS version 17.0 statistical package was used to analyze the data, and ANOVA analysis followed by LSD's method was employed to understand the variations in data.

2.4. Dynamic adsorption equilibrium

Pseudo-first-order kinetic, pseudo-second-order kinetic, and intraparticle diffusion models were used to determine the adsorption mechanisms of Cd(II) onto HA-TiO₂. The pseudo-first-order kinetic model (1) is expressed in the exponential form and the pseudo-second-order kinetic model (2) is described in the hyperbola form [34]:

$$q_t = q_e(1 - e^{-k_1 t}) \quad (1)$$

$$q_t = \frac{t k_2 q_e^2}{1 + t k_2 q_e} \quad (2)$$

where k_1 and k_2 are the rate constants of adsorption (mg μg⁻¹ min⁻¹) for the pseudo-first-order and pseudo-second-order models, respectively; q_t is the amount of Cd(II) adsorbed at time t (μg mg⁻¹); q_e is the amount of Cd(II) adsorbed at equilibrium (μg mg⁻¹); and k_2 and q_e can be calculated from the slope and intercept of the plot of t/q_t vs. t . The initial adsorption rate (v_0) can be estimated as follows:

$$v_0 = k_2 q_e^2 \quad (3)$$

Parameter q_t is calculated according to:

$$q_t = (C_0 - C_t) \times V/m \quad (4)$$

where C_0 and C_t are the concentrations (mg L^{-1}) of Cd(II) before adsorption and at any time t , respectively. In addition, m is the mass of the adsorbent (mg), and V is the volume of the suspension in each experimental tube (L).

The intraparticle diffusion kinetic model is used to determine the rate-limiting step if there is a possibility of intraparticle diffusion in the adsorption process. The equation for this model is as follows [35]:

$$q_t = k_{\text{int}} t^{0.5} + C \quad (5)$$

where k_{int} ($\text{mg g}^{-1} \text{min}^{-0.5}$) is the intraparticle diffusion rate constant, and C ($\mu\text{g mg}^{-1}$) is the constant proportional to the extent of boundary layer thickness.

3. Results and discussion

3.1. Behavior of Cd(II) in the ternary system

Fig. 1 shows Cd(II) adsorption by different adsorbents under a range of conditions. From the figure, it is clear that HA exhibits the highest adsorption capacity for Cd(II), as the abundant functional groups on HA can interact with metal ions to form stable complexes. TiO_2 also shows some adsorption activity for Cd(II) ions in solution for two main reasons. Firstly, nano- TiO_2 has a high specific surface area, this property of nano- TiO_2 make the Cd(II) ions can be adsorbed on the nano- TiO_2 . Secondly, the surface charge of nano- TiO_2 is negative at pH 8 (Fig. 2), thus

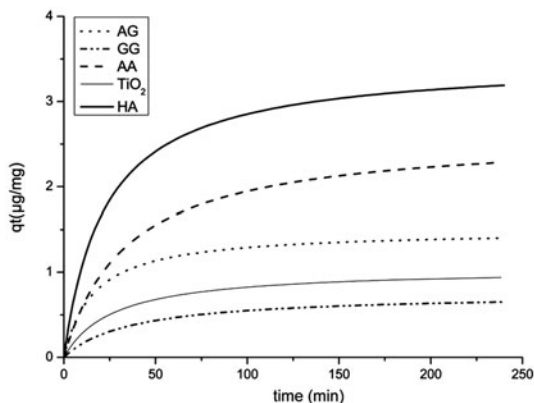


Fig. 1. Pseudo-second-order models of Cd(II) adsorption under different conditions (GG, AA, and AG used HA- TiO_2 as adsorbents). For GG, the experiments were carried out under solar irradiation. For AA, the experiments were carried out in the absence of solar irradiation. For AG, Cd(II) adsorption was carried out under solar irradiation, while the attachment experiment was carried out in the absence of solar irradiation.

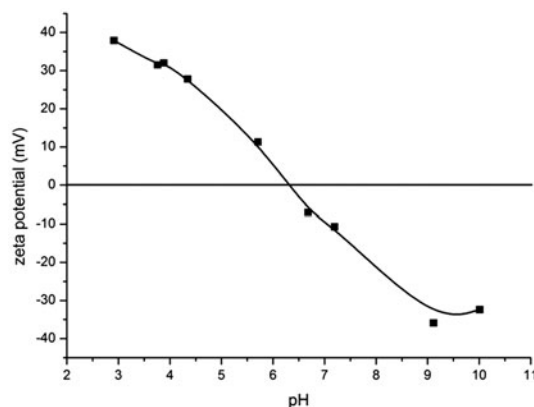


Fig. 2. The zeta potential of nano- TiO_2 as a function of pH.

promoting the adsorption of positively charged Cd(II) ions. However, nano- TiO_2 has the weakest capacity for Cd(II) adsorption under all conditions studied. After the adsorption of HA onto the surface of nano- TiO_2 (group AA, the experiments were carried out in the absence of solar irradiation), it facilitated the adsorption of Cd(II) significantly because of the complexation between HA and Cd(II) ions. When solar irradiation is introduced into the experiment, significant differences ($p < 0.05$) in Cd(II) adsorption are observed. In the case of group AG, HA is fixed onto nano- TiO_2 without solar irradiation, and then the particles are collected and used to adsorb Cd(II) ions under solar irradiation. In this situation, the Cd(II) adsorption capacity is lower than that of group AA. We suppose the HA adsorbed onto the nano- TiO_2 is partially decomposed under solar irradiation. However, the Cd(II) adsorption in group AG is higher than that of pure TiO_2 . Maybe, the complexation between HA and Cd(II) ions would protect the HA from complete decomposition. Indeed, in the case of both HA adsorption and Cd(II) adsorption, which are carried out under solar irradiation (group GG, the experiments were carried out under solar irradiation), the Cd(II) adsorption is lower than that of pure TiO_2 . The results illustrates that solar irradiation in both processes affect the Cd(II) adsorption apparently. It can be attributed to the reason that solar irradiation on the photoactive nano- TiO_2 degraded the adsorbed HA into byproducts. And these byproducts occupy the adsorption sites for Cd(II) adsorption on the nano- TiO_2 . Based on the above results, detailed adsorption processes for Cd(II) adsorption by TiO_2 is proposed and shown in Fig. 3.

Table 1 lists the kinetic parameters for the adsorption of Cd(II). The correlation coefficients of the pseudo-first-order model range between 0.731 and

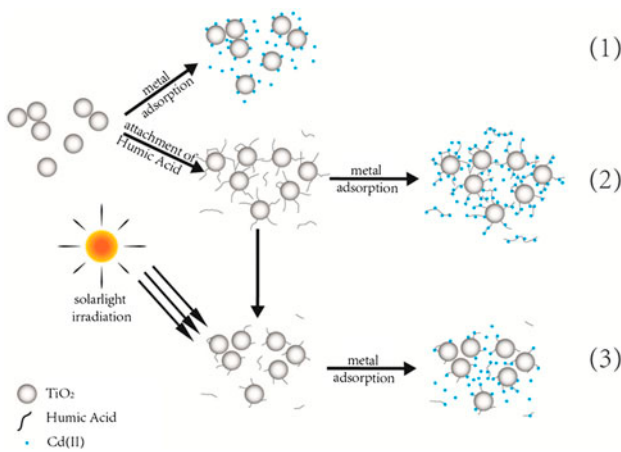


Fig. 3. Cd(II) adsorption by TiO₂ in aqueous systems. Notes: (1) Cd(II) adsorption by TiO₂, (2) attachment of HA to TiO₂, and subsequent adsorption of Cd(II) without solar irradiation, and (3) attachment of HA to TiO₂, and subsequent adsorption of Cd(II) under solar irradiation.

0.914, which are lower than that of the pseudo-second-order model. This suggests that the pseudo-second-order model is the more appropriate model for our studies. Similar results were also reported by other groups [33,36–38]. In this case, the better fit of the pseudo-second-order model indicates that the adsorption capacity of Cd(II) is proportional to the number of active sites on the adsorbents [33]. The pseudo-second-order model also has a number of benefits, as it is capable of evaluating the capacity of effective adsorption, the rate of initial adsorption, and the rate constant, without inputting any further parameters [39]. It is evident from the above results

that the adsorption efficiencies for Cd(II) increase sharply within half an hour under all sets of conditions studied. The highest initial adsorption rate is observed for HA, likely due to the large amount of active sites available [40]. When HA is attached onto nano-TiO₂, the initial adsorption rate increases because of the active sites supplied by HA. However, the solar irradiation causes the degradation of HA thus decreases the amount of functional groups. Therefore, the initial sorption rates of group AG and GG decreased. The adsorption of Cd(II) approaches equilibrium as the process lasting. The available active adsorption sites, which mainly determined the rate of the Cd(II) adsorption [33], decline by solar light irradiation. Besides, the electrostatic repulsion between positively charged metals adsorbed onto nano-TiO₂ and free metal ions in solution inhibited the continued adsorption of metal ions [41]. In addition, the slow pore diffusion of metal ions into adsorbents could also decrease the uptake rate [36]. We therefore consider an appropriate contact time of 240 min to allow equilibrium to be reached in the adsorption of Cd(II). Similar results have been reported by other groups [33]. In addition, the correlation coefficients of the intraparticle diffusion model ranged from 0.854 to 0.988, with no lines passing through the origin since the values of C are not equal to zero. It means that the intraparticle diffusion model was not the rate-limiting step for metal adsorption in the present condition [35].

3.2. Analysis of binding mechanisms

The presence of HA in the aqueous system has been found to affect the adsorption behavior of both

Table 1

Kinetic parameters for the adsorption of Cd(II) by complex materials (GG, AA, and AG used HA-TiO₂ as adsorbents). For GG, the experiments were carried out under solar irradiation. For AA, the experiments were carried out in the absence of solar irradiation. For AG, Cd(II) adsorption was carried out under solar irradiation, while the attachment experiment was carried out in the absence of solar irradiation

Kinetic models		HA	AA	AG	GG	TiO ₂
Pseudo-first-order kinetic model	q_e ($\mu\text{g mg}^{-1}$)	3.075	2.255	1.359	0.629	906
	k_1 (min^{-1})	0.033	0.022	0.043	0.025	0.027
	R^2	0.896	0.895	0.914	0.781	0.731
Pseudo-second-order kinetic model	q_e ($\mu\text{g mg}^{-1}$)	3.485	2.609	1.494	0.750	1.047
	k_2 ($\text{mg } \mu\text{g}^{-1} \text{min}^{-1}$)	0.013	0.011	0.042	0.036	0.035
	v_0 ($\mu\text{g mg}^{-1} \text{min}^{-1}$)	0.157	0.077	0.094	0.020	0.039
	R^2	0.943	0.903	0.886	0.755	0.771
Intraparticle diffusion model	k_{int} ($\mu\text{g mg}^{-1} \text{min}^{0.5}$)	0.206	0.146	0.089	0.042	0.069
	C ($\mu\text{g mg}^{-1}$)	0.531	0.310	0.230	0.059	0.104
	R^2	0.921	0.885	0.676	0.771	0.629

metals and nanoparticles [42–44] because of two main reasons. Firstly, the multifunctional polydisperse HA adsorbed onto nano-TiO₂ is capable of inhibiting aggregation by affecting the particle–particle interactions in the composite colloidal reaction medium [45]. Dispersion of nanoparticles in the aqueous system can result in higher mobility and thus facilitates the movement of contaminant adsorbed on the nanoparticles [46]. Secondly, the polyanionic organic HA attached onto the nanoparticles can also alter the surface properties of the nanoparticles [47,48], including surface charge and functional groups. This would promote metal complexation because of the formation of cation bridges between positively charged metal ions and negatively charged functional groups (e.g. –OH, –NH₂, and –COOH) of HA [41,49]. An increase in Cd (II) adsorption in the group AA confirms the mechanism outlined above. The interactions between metals, nano-TiO₂, and HA are determined by a range of mechanisms involving surface complexation reactions, Coulombic electrostatic interactions, and Van der Waals forces. These mechanisms may occur simultaneously, thus leading to a rather complex reaction mechanism [50]. Considering the photoactivity of TiO₂, we investigated the effects of solar irradiation on the process. After solar irradiation, the HA molecules are transformed to new entities before complete mineralization [51]. The different Cd(II) adsorptions observed in AG and GG groups confirm that solar irradiation indeed affects the Cd(II) adsorption behavior of nano-TiO₂. To determine more specifically the influence of solar irradiation, we studied the changes in both solution and HA-TiO₂ during attachment experiments.

It has been previously reported that the UV–vis spectra of HA are generally broad and featureless, and decrease in intensity with increasing wavelength [52]. The UV absorbance at 254 nm and TOC were measured as substitution parameters to represent the NOM content in natural waters [53]. Only 13.7% of HA is removed from the solution in group A, which is much lower than that removed in group G (Table 2). It is due to the fact that TiO₂-generated active oxygen species (such as hydroxyl radicals (·OH), superoxide radicals (O₂^{·-}), hydrogen peroxide (H₂O₂), or singlet

oxygen) attacks and decomposes HA molecules under solar irradiation. However, HA also played an important role in the production of ·OH and O₂^{·-} by TiO₂ under solar light irradiation due to the following two reasons [54]. Firstly, HA acts as electron donor and acceptor, and thus promotes the production of O₂^{·-}. Secondly, HA can also block the light absorption of TiO₂ and decrease the production of ·OH [54]. Especially, the alkaline condition in attachment experiments would cause the HA molecules to open, the acidic functional groups on the HA molecules would be deprotonated. Furthermore, the number of hydrogen bonds decreased and the repellent negative charges increased. These factors made the humic molecules more susceptible to attack by ·OH radicals [55]. Additionally, as the humic molecules generally contained a large amount of aromatic sites with high electron density, the hydroxyl radicals were also prone to attack these sites [56]. In the absence of solar irradiation, the HA just attaches onto nano-TiO₂ without further deformation. In our study, the removal of HA in group A is much lower than the level of 40%. As the attachment of HA on oxide surfaces was largely pH dependent, the amount of attachment rapidly increased with decreasing pH [57,58]. In alkaline solutions, the acidic functional groups on HA are deprotonated and negatively charged. Therefore, the adsorption of HA is strongly inhibited owing to the electrostatic repulsion [59].

It has previously been reported that UV absorbance at 203 nm and 254 nm represented an estimation of the degree of functionality of the aromatic ring [60]. The ratio E₂₅₀/E₃₆₅ is related to the molecular size and aromaticity of the HSs [61]. The ratio E₄₆₅/E₆₆₅ is highly related to the humification degree (decomposition of organic matter (OM)) and molecular weight of OM [62]. From Table 2, it can be seen that the UV–vis ratios of E₂₅₀/E₃₆₅ in group A are comparable to those of the original HA solution, as there is no chemical transformations taking place for the HA molecules. However, the ratios of E₂₅₀/E₃₆₅ calculated for the solution in group G varied obviously. The lower E₂₅₄/E₂₀₃ ratio indicates that the number of hydroxyl, carbonyl, ester, and carboxylic groups

Table 2

Parameters of the original solutions after attachment experiments (HA = humic acid, A = no solar irradiation used and G = solar irradiation used)

	UV ₂₅₄ removal (%)	TOC (mg L ⁻¹)	E ₂₅₀ /E ₃₆₅	E ₂₅₄ /E ₂₀₃	E ₄₆₅ /E ₆₆₅
HA	–	156.99	2.44	1.05	5.88
A	13.70	82.40	2.36	0.98	6.52
G	44.13	91.89	5.96	0.59	1.47

decreases, while an increase in the E250/E365 ratio indicates that the molecular size of HA decreases. This is owing to stimulation of photoactive nano-TiO₂ by solar irradiation, resulting in the consumption of the acidic groups of HA. Thus, new entities with smaller molecular size are formed and released into solution. A low E465/E665 ratio for group G confirms this hypothesis.

From the TOC analysis, it can be seen that the percent of residual TOC in group A is lower than that of group G. However, the percent of residual HA in group A is higher than that of group G. The difference can be ascribed to the following reasons. In group A, the removal of TOC is mainly caused by the adsorption of HA by TiO₂. However, in group G, the removal of TOC is caused by the adsorption and degradation of HA by TiO₂. Furthermore, HA can be decomposed into new byproducts before total mineralization in group G. Most of these byproducts may release into the solution, and give rise to a higher TOC value. As UV-vis spectroscopy measures only the intensity of HA in solution, the intensity of HA reduces as the reactions proceeds. Because the decomposition takes place in group G, it is observed that HA is removed more in group G than in group A.

3.3. Structural change of HA-TiO₂

FTIR was used to elucidate the different structural domains present in each solid material after the attachment processes, and the results are shown in Fig. 4. For the spectrum of HA, the wide band around

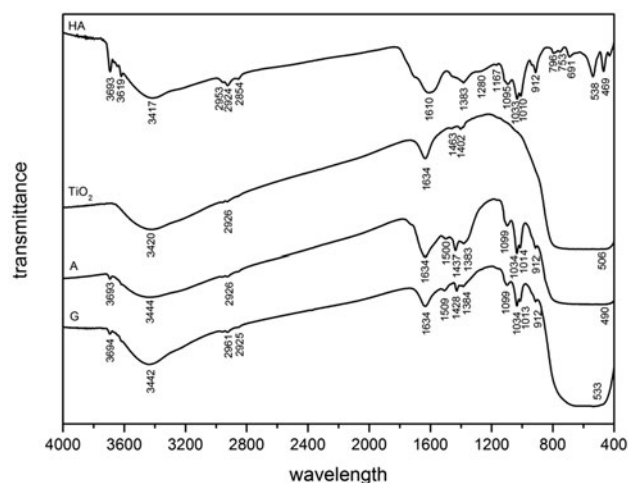


Fig. 4. FTIR spectrum of solid materials after the attachment process (HA = humic acid, A = no solar irradiation used and G = solar irradiation used).

3,400 cm⁻¹ corresponds to the stretching vibrations of O–H and N–H. The bands around 2,900 cm⁻¹ correspond to aliphatic C–H, C–H₂, and C–H₃ stretching. The signal corresponding to the stretching vibration of the carboxylic groups is observed at approximately 1,700 cm⁻¹, with additional bands around 1,610 cm⁻¹ corresponding to the stretching vibrations of aromatic C=C moieties, quinone C=O and/or C=O H-bonded conjugated ketones and symmetric stretching of COO⁻ groups [63]. The band at approximately 1,460 cm⁻¹ corresponds to the bending vibration of aliphatic C–H groups. A broad band of medium intensity between 1,410 and 1,380 cm⁻¹ can be assigned to a number of transformations, namely the O–H deformation and C–O stretching of phenolic OH groups, C–H deformation of CH₂ and CH₃ groups, and/or antisymmetric stretching of COO⁻ groups. The band centered at 1,095 cm⁻¹ is ascribed to the C–O moiety of the alcohol and ether groups, whereas the C–O stretching of polysaccharides (or polysaccharide-like substances) is observed in the bands close to 1,020 cm⁻¹. Finally, the peaks observed between 910 and 665 cm⁻¹ are attributed to aromatic C–H out-of-plane bending vibrations. As can be seen in Fig. 4, the spectrum of nano-TiO₂ shows fewer number of bands than HA. The broad band at 3,420 cm⁻¹ can be attributed to the primary O–H stretch of the hydroxyl functional group, and that at approximately 1,630 cm⁻¹ is attributed to the bending vibration of the H–OH groups. Finally, the band observed between 800 and 420 cm⁻¹ corresponds to the Ti–O bending of nano-TiO₂ [64].

From the FTIR information reported above, it is clear that the spectrum of HA confirms the presence of phenolic and hydroxylic groups, carboxylic groups, alkanes, aliphatic amines, and ethers, along with the carbon–carbon double bonds. Peaks corresponding to Ti–O bonds and hydroxyl groups are observed in the spectrum of nano-TiO₂. It can also be seen that several functional groups had been successfully introduced onto nano-TiO₂ after further examination of the spectrum. Furthermore, the intensity of peaks present in the 1,600–1,650 cm⁻¹ region enhances. It indicates that aromatic oxygen-containing moieties were introduced onto the surface [33]. After the adsorption of aliphatic carbon fractions, the intensity of the peak at approximately 2,900 cm⁻¹ increases. The disappearance of peak at 1,280 cm⁻¹ may be due to the strong interactions of the phenolic OH group with nano-TiO₂ surfaces [57]. Indeed, a significant shift for the peak of the aromatic C=C stretch from 1,600 cm⁻¹ in HA to 1,500 cm⁻¹ in HA-TiO₂ indicates strong interactions of phenolic OH group with nano-TiO₂ [65]. The hydrogen bonding between the acidic groups of HA and the hydroxyl groups on the nanoparticles is believed to

play an essential role in HA adsorption onto nano-TiO₂ [66]. In addition, several studies have shown that oxide and aluminosilicate mineral surfaces are capable of adsorbing linear, threadlike polysaccharides [67–69]. Thus, the Cd(II) adsorption capacity of group A improved significantly after the introduction of functional groups on the TiO₂ surface.

Fig. 5 shows the scanning electron microscope (SEM) images of the TiO₂ nanoparticles and HA-TiO₂ during attachment experiments. The bare TiO₂ nanopowder (Fig. 5(a)) is composed of spherical nanoparticles with distinct boundary. The primary particle size of nano-TiO₂ is quite uniform in about 20 nm. Compared with bare TiO₂, the particles in group A (Fig. 5(b)) became more densely clustered. Due to the HA covered around the nanoparticles, the boundary of the nanoparticles became nebulous, and the particles gather into larger aggregates. Furthermore, many HAs can be seen clearly (marked by arrows). In the group G (Fig. 5(c)), we find that the nanoparticles distributed like bare TiO₂, the boundary of the nanoparticles becomes clearer than that of group A. However, it still shows that some particles are covered by the OMs. Based on the results, the HA adsorbed on TiO₂ nanoparticles changes the surface property of the particles, thus influencing the Cd(II) adsorption. The solar irradiation induces the decomposition of HA by TiO₂ due to the generation of active oxygen species, thus some fragments or new entities of HA remain on the surface of the TiO₂. We infer that these OMs may also influence the Cd(II) adsorption.

Further examination of the FTIR spectrum of HA reveals that solar irradiation results in a decline in the intensity of the peaks corresponding to the HA functional groups. Compared with group A, the intensity of group G is weaker, in particular in the fingerprint region. The weaker intensity of group G demonstrates that HA is decomposed into unknown entities under solar irradiation, thus causing the TOC value in group G to be higher than that of group A. Major changes in intensity are observed between 1,380 and 1,650 cm⁻¹, which correspond to the O–H deformation and C–O stretching of the phenolic OH groups. As it is expected that the principal binding moiety between HA and nano-TiO₂ should be the hydroxyl group, these observations support this hypothesis. In addition, these reactions, caused by the effects of solar irradiation on the hydroxyl groups, are the main reason for the generation of the more favorable ·OH radical via the hole oxidation of –OH [70]. According to a number of other studies [57,71], we expect that the surplus active sites present on the nano-TiO₂ surface would combine with the C–O functional groups of HA after all OH groups are exhausted. Indeed, this is

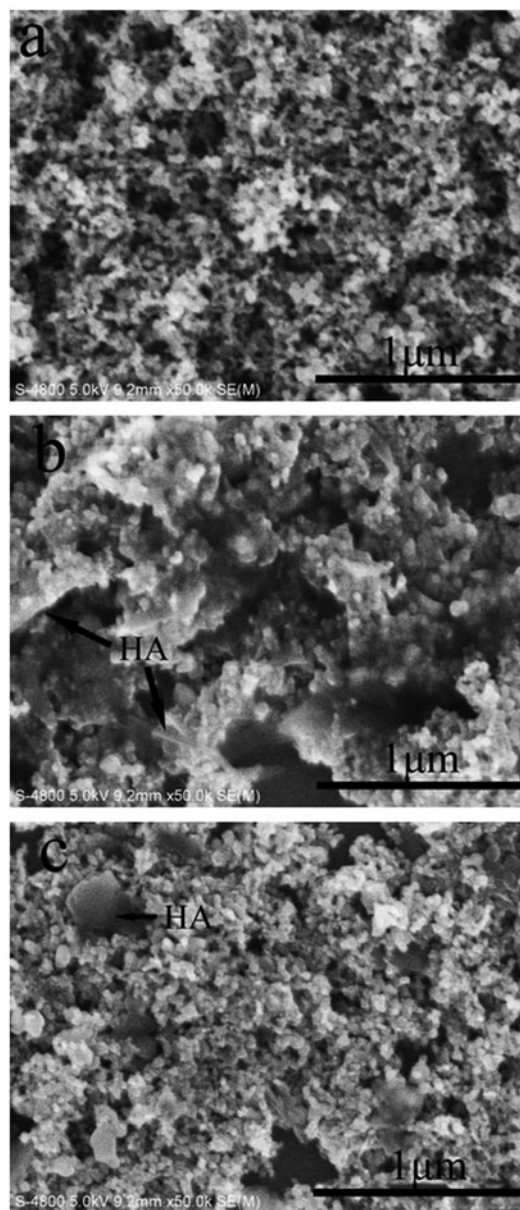


Fig. 5. SEM images of (a) TiO₂ nanoparticles, (b) HA-TiO₂ complex without solar irradiation (group A), and (c) HA-TiO₂ complex under solar irradiation (group G).

supported by a decrease in the intensity of the peaks at 1,095 and 1,020 cm⁻¹ in group G. As the functional groups are more abundant in group A than in group G, a greater amount of Cd(II) adsorption is observed in the AA and AG group compared to that in the GG group. The FTIR spectrum of group G shows that it has more functional groups than TiO₂. We thus propose that the HA is decomposed into some byproducts, and these byproducts are adsorbed on the TiO₂.

In order to determine changes in the functional group that take place with Cd(II) adsorption under

solar irradiation, we use FTIR to analyze the solid materials after Cd(II) adsorption. Fig. 6 shows the differences in the FTIR spectra of solid materials before and after Cd(II) adsorption. The bands located in the fingerprint area change significantly after Cd(II) adsorption. As solar light is abundant in nature, it is still capable of stimulating the photoactive nano-TiO₂ even when the nanoparticles have been coated with HA. We also find that the HA enhanced the absorption ability of TiO₂ for visible light (Fig. 7). In fact, HA can act as photosensitizer for injecting electrons from their excited state to the conduction band of TiO₂ [72]. We observe that the polysaccharides (or polysaccharide-like substances), aromatic rings, and phenolic hydroxyl groups are oxidized into alkanes or other unknown entities during the process. According to many studies [73–77], the carboxylic and hydroxyl groups (both aromatic and aliphatic) are capable of complexing metal ions. From our results, we can therefore confirm the significant decline in the number of hydroxyl groups under solar irradiation, which is likely to be the main reason for the differences in Cd(II) adsorption between the AG and AA groups. Maybe, the complexation between Cd(II) ions and HA prevents the complete decomposition of HA by TiO₂, thus ensuring a higher Cd(II) adsorption capacity for the AG group compared to pure TiO₂. After Cd(II) adsorption, the functional groups in group GG-Cd are more abundant than that of pure TiO₂. Because the HA is decomposed into byproducts at first step, and

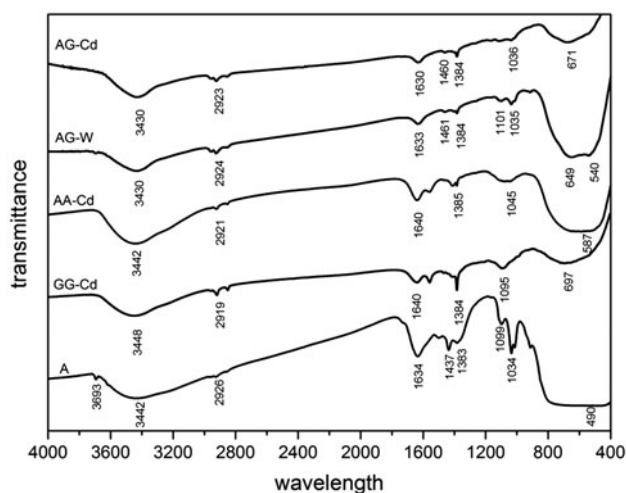


Fig. 6. FTIR spectrum of group A and G after Cd(II) adsorption. The GG-Cd and AG-Cd spectrum was collected from the Cd(II) solution under solar irradiation. The AA-Cd spectrum was collected from the Cd(II) solution without solar irradiation. The spectrum of AG-W was collected from the aqueous phase.

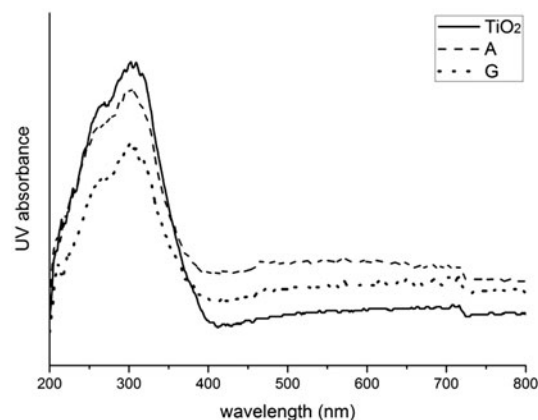


Fig. 7. UV-visible diffuse reflectance spectra of TiO₂, group A and group G.

bonds to the TiO₂, we propose that the functional groups on the byproducts could not adsorb the Cd(II). Thus, causing the Cd(II) adsorption lower than that of pure TiO₂.

After Cd(II) adsorption, the intensities of the broad peaks at approximately 800 and 420 cm⁻¹ in group GG-Cd and AG-Cd declined obviously. Because of the decomposition of HA, the adsorption sites on TiO₂ re-expose in solution and adsorb free Cd(II) ions. In group AA-Cd, obviously broad peaks at approximately 800 and 420 cm⁻¹ can be observed. It confirms that the main Cd(II) adsorption is caused by HA. In addition, a strong and pointed band at 1,385 cm⁻¹ appears in group GG-Cd. It is consistent with a -COO-metal stretching reported by Ou [58]. Similar result can be seen between group AG-Cd and group AG-W. In an alternative situation, metal ions can be adsorbed by forming ligand-bridging ternary surface complexes (M-HA-S), or surface complexes in which the metal ion directly bonds to functional groups on the nanoparticles. In addition, binary M-S or metal-bridging ternary surface complexes (HA-M-S) can form, where S represents the adsorption site on the solid surface, and M is the metal ion [78]. We also confirm that the hydroxyl group on HA plays an important role in complexing Cd(II) and nano-TiO₂. This can explain why the adsorption capacities of Cd(II) in the AG and AA groups are between those of HA and nano-TiO₂, as their binding sites contain many similarities. Therefore, based on the information above, we can propose that the key structures in our study are likely to be M-HA-TiO₂ and M-TiO₂. Based on this information, the process by which solar irradiation can affect Cd(II) adsorption is determined to be the degradation of the functional group remaining on nano-TiO₂.

4. Conclusion

In the present work, we investigated the Cd(II) adsorption by nano-TiO₂ in the presence of HA under a range of conditions. The attachment of HA onto nano-TiO₂ resulted in an increase in Cd(II) adsorption because of the participation of functional groups of HA in the adsorption process. However, it was found that solar irradiation resulted in a decrease in Cd(II) adsorption by nano-TiO₂ because of decomposition of the attached HA. In addition, the photoactive nano-TiO₂ induced the conversion of HA macromolecules into new byproducts under solar irradiation. Some byproducts occupied the sites of nano-TiO₂, and caused the lower Cd(II) adsorption ability. It can be ascribed to a decrease in the amount of hydroxyl groups of these byproducts since the hydroxyl groups are the main sites for Cd(II) adsorption. Based on the above results, it is expected that the bioavailability and toxicity of heavy metals would be altered when photoactive nanoparticles enter into aquatic system.

Acknowledgment

This work was supported by a grant from National Science Funds for Creative Research Groups of China (No. 51421006), National Science Funds for Distinguished Young Scholars (No. 51225901), The National Science Foundation of China for Excellent Young Scholars (No. 51422902), Program for Changjiang Scholars and Innovative Research Team in University (No. IRT13061), The Key Program of National Science Foundation of China (No. 41430751), The National Natural Science Foundation of China (No. 51479065) and PAPD.

References

- [1] F. Fu, Q. Wang, Removal of heavy metal ions from wastewaters: A review, *J. Environ. Manage.* 92 (2011) 407–418.
- [2] M.L.S. Oliveira, C.R. Ward, D. French, J.C. Hower, X. Querol, L.F.O. Silva, Mineralogy and leaching characteristics of beneficiated coal products from Santa Catarina, Brazil, *Int. J. Coal Geol.* 94 (2012) 314–325.
- [3] X.D. Li, S.L. Lee, S.C. Wong, W.Z. Shi, Iain Thornton, The study of metal contamination in urban soils of Hong Kong using a GIS-based approach, *Environ. Pollut.* 129 (2004) 113–124.
- [4] M. Chabukdhara, A.K. Nema, Assessment of heavy metal contamination in Hindon River sediments: A chemometric and geochemical approach, *Chemosphere* 87 (2012) 945–953.
- [5] H. Liu, L. Li, C. Yin, B. Shan, Fraction distribution and risk assessment of heavy metals in sediments of Moshui Lake, *J. Environ. Sci.* 20 (2008) 390–397.
- [6] A. Dong, S. Zhai, M. Zabel, Z. Yu, H. Zhang, F. Liu, Heavy metals in Changjiang estuarine and offshore sediments: Responding to human activities, *Acta Oceanolog. Sin.* 31 (2012) 88–101.
- [7] C. Christophoridis, D. Dedepsidis, K. Fytianos, Occurrence and distribution of selected heavy metals in the surface sediments of Thermaikos Gulf, N. Greece. Assessment using pollution indicators, *J. Hazard. Mater.* 168 (2009) 1082–1091.
- [8] Y. Qiao, H. Pan, Y. Yang, J. Gu, J. Zhao, Distribution and accumulation of heavy metals in surface sediments from a subtropical bay affected by the Special Economic Zone, China, *Water Sci. Technol.* 67 (2013) 2009–2016.
- [9] P. Li, X. Wang, G. Allinson, X. Li, X. Xiong, Risk assessment of heavy metals in soil previously irrigated with industrial wastewater in Shenyang, China, *J. Hazard. Mater.* 161 (2009) 516–521.
- [10] P. Rath, U.C. Panda, D. Bhatta, K.C. Sahu, Use of sequential leaching, mineralogy, morphology and multivariate statistical technique for quantifying metal pollution in highly polluted aquatic sediments—A case study: Brahmani and Nandira Rivers, India, *J. Hazard. Mater.* 163 (2009) 632–644.
- [11] C.R. Evanko, D.A. Dzombak, Remediation of metals-contaminated soils and groundwater, Ground-water remediation technologies analysis center, 485 (1997) 3–22.
- [12] O. Polvillo, J.A. González-Pérez, T. Boski, F.J. González-Vila, Structural features of humic acids from a sedimentary sequence in the Guadiana estuary (Portugal–Spain border), *Org. Geochem.* 40 (2009) 20–28.
- [13] Y.S.S. Al-Faiyz, CPMAS 13C NMR characterization of humic acids from composted agricultural Saudi waste, *Arab. J. Chem.* (in press), doi: 10.1016/j.arabjc.2012.12.018.
- [14] J.M. De la Rosa, M. Santos, M.F. Araújo, Metal binding by humic acids in recent sediments from the SW Iberian coastal area, *Estuarine Coastal Shelf Sci.* 93 (2011) 478–485.
- [15] M. Halim, P. Conte, A. Piccolo, Potential availability of heavy metals to phytoextraction from contaminated soils induced by exogenous humic substances, *Chemosphere* 52 (2003) 265–275.
- [16] B. El-Eswed, F. Khalili, Adsorption of Cu(II) and Ni(II) on solid humic acid from the Azraq area, Jordan, *J. Colloid Interface Sci.* 299 (2006) 497–503.
- [17] Z.R. Komy, A.M. Shaker, S.E.M. Heggy, M.E.A. El-Sayed, Kinetic study for copper adsorption onto soil minerals in the absence and presence of humic acid, *Chemosphere* 99 (2014) 117–124.
- [18] B. Scaglia, F. Tambone, F. Adani, Cr(VI) reduction capability of humic acid extracted from the organic component of municipal solid waste, *J. Environ. Sci.* 25 (2013) 487–494.
- [19] B. Nowack, T.D. Bucheli, Occurrence, behavior and effects of nanoparticles in the environment, *Environ. Pollut.* 150 (2007) 5–22.
- [20] R. Kaegi, A. Ulrich, B. Sinnet, R. Vonbank, A. Wichser, S. Zuleeg, H. Simmler, S. Brunner, H. Vonmont, M. Burkhardt, M. Boller, Synthetic TiO₂ nanoparticle emission from exterior facades into the aquatic environment, *Environ. Pollut.* 156 (2008) 233–239.

- [21] W.-X. Zhang, Nanoscale iron particles for environmental remediation: An overview, *J. Nanopart. Res.* 5 (2003) 323–332.
- [22] G.V. Lowry, K.M. Johnson, Congener-specific dechlorination of dissolved PCBs by microscale and nanoscale zerovalent iron in a water/methanol solution, *Environ. Sci. Technol.* 38 (2004) 5208–5216.
- [23] J. Schmidt, W. Vogelsberger, Aqueous long-term solubility of titania nanoparticles and titanium (IV) hydrolysis in a sodium chloride system studied by adsorptive stripping voltammetry, *J. Solution Chem.* 38 (2009) 1267–1282.
- [24] R.A. French, A.R. Jacobson, B. Kim, S.L. Isley, R.L. Penn, P.C. Baveye, Influence of ionic strength, pH, and cation valence on aggregation kinetics of titanium dioxide nanoparticles, *Environ. Sci. Technol.* 43 (2009) 1354–1359.
- [25] X. Zhang, H. Sun, Z. Zhang, Q. Niu, Y. Chen, J.C. Crittenden, Enhanced bioaccumulation of cadmium in carp in the presence of titanium dioxide nanoparticles, *Chemosphere* 67 (2007) 160–166.
- [26] X. Chen, S.S. Mao, Titanium dioxide nanomaterials: Synthesis, properties, modifications, and applications, *Chem. Rev.* 107 (2007) 2891–2959.
- [27] M. Cristina Yeber, J. Rodríguez, J. Freer, N. Durán, H.D. Mansilla, Photocatalytic degradation of cellulose bleaching effluent by supported TiO₂ and ZnO, *Chemosphere* 41 (2000) 1193–1197.
- [28] M. Rajca, M. Bodzek, Kinetics of fulvic and humic acids photodegradation in water solutions, *Sep. Purif. Technol.* 120 (2013) 35–42.
- [29] J.K. Yang, S.M. Lee, Removal of Cr(VI) and humic acid by using TiO₂ photocatalysis, *Chemosphere* 63 (2006) 1677–1684.
- [30] J.C. Wasserman, F.B.L. Oliveira, M. Bidarra, Cu and Fe associated with humic acids in sediments of a tropical coastal lagoon, *Org. Geochem.* 28 (1998) 813–822.
- [31] A.K. Pandey, S.D. Pandey, V. Misra, Stability constants of metal-humic acid complexes and its role in environmental detoxification, *Ecotoxicol. Environ. Saf.* 47 (2000) 195–200.
- [32] E.B.Ö. Güngör, M. Bekbolet, Zinc release by humic and fulvic acid as influenced by pH, complexation and DOC sorption, *Geoderma* 159 (2010) 131–138.
- [33] Q. Chen, D. Yin, S. Zhu, X. Hu, Adsorption of cadmium(II) on humic acid coated titanium dioxide, *J. Colloid Interface Sci.* 367 (2012) 241–248.
- [34] L.S. Zur, Theorie der Sogenannten Adsorption Gelöster Stoffe, *K. Sven. Vetenskapskad. Handl.* 24 (1898) 1–39.
- [35] W. Weber, J. Morris, Kinetics of adsorption on carbon from solution, *J. Sanit. Eng. Div. Am. Soc. Civ. Eng.* 89 (1963) 31–60.
- [36] L. Xiong, C. Chen, Q. Chen, J. Ni, Adsorption of Pb(II) and Cd(II) from aqueous solutions using titanate nanotubes prepared via hydrothermal method, *J. Hazard. Mater.* 189 (2011) 741–748.
- [37] Y.-S. Ho, G. McKay, The kinetics of sorption of divalent metal ions onto sphagnum moss peat, *Water Res.* 34 (2000) 735–742.
- [38] Y.-S. Ho, G. McKay, Pseudo-second order model for sorption processes, *Process Biochem.* 34 (1999) 451–465.
- [39] Y.-S. Ho, A.E. Ofomaja, Pseudo-second-order model for lead ion sorption from aqueous solutions onto palm kernel fiber, *J. Hazard. Mater.* 129 (2006) 137–142.
- [40] M. Rafatullah, O. Sulaiman, R. Hashim, A. Ahmad, Adsorption of copper (II), chromium (III), nickel (II) and lead (II) ions from aqueous solutions by meranti sawdust, *J. Hazard. Mater.* 170 (2009) 969–977.
- [41] T. Wang, W. Liu, L. Xiong, N. Xu, J. Ni, Influence of pH, ionic strength and humic acid on competitive adsorption of Pb(II), Cd(II) and Cr(III) onto titanate nanotubes, *Chem. Eng. J.* 215–216 (2013) 366–374.
- [42] J.A. Davis, R. Gloor, Adsorption of dissolved organics in lake water by aluminum oxide. Effect of molecular weight, *Environ. Sci. Technol.* 15 (1981) 1223–1229.
- [43] E. Tipping, D. Cooke, The effects of adsorbed humic substances on the surface charge of goethite (α -FeOOH) in freshwaters, *Geochim. Cosmochim. Acta* 46 (1982) 75–80.
- [44] A. Vermeer, W. van Riemsdijk, L. Koopal, Adsorption of humic acid to mineral particles. 1. Specific and electrostatic interactions, *Langmuir* 14 (1998) 2810–2819.
- [45] B.J.R. Thio, D. Zhou, A.A. Keller, Influence of natural organic matter on the aggregation and deposition of titanium dioxide nanoparticles, *J. Hazard. Mater.* 189 (2011) 556–563.
- [46] T. Kanti Sen, K.C. Khilar, Review on subsurface colloids and colloid-associated contaminant transport in saturated porous media, *Adv. Colloid Interface Sci.* 119 (2006) 71–96.
- [47] E. Illés, E. Tombácz, The role of variable surface charge and surface complexation in the adsorption of humic acid on magnetite, *Colloids Surf., A: Physicochem. Eng. Aspects* 230 (2003) 99–109.
- [48] E. Illés, E. Tombácz, The effect of humic acid adsorption on pH-dependent surface charging and aggregation of magnetite nanoparticles, *J. Colloid Interface Sci.* 295 (2006) 115–123.
- [49] G. Yuan, B. Xing, Effects of metal cations on sorption and desorption of organic compounds in humic acids, *Soil Sci.* 166 (2001) 107–115.
- [50] S. Sen Kavurmaci, M. Bekbolet, Photocatalytic degradation of humic acid in the presence of montmorillonite, *Appl. Clay Sci.* 75–76 (2013) 60–66.
- [51] M. Bekbolet, F. Cecen, G. Ozkosemen, Photocatalytic oxidation and subsequent adsorption characteristics of humic acids, *Water Sci. Technol.* 34 (1996) 65–72.
- [52] C.S. Uyguner, M. Bekbolet, Evaluation of humic acid photocatalytic degradation by UV-vis and fluorescence spectroscopy, *Catal. Today* 101 (2005) 267–274.
- [53] I.N. Najm, N.L. Patania, J.G. Jacangelo, S.W. Krasner, Evaluating surrogates for disinfection by-products, *J. Am. Water Works Assoc.* 86 (1994) 98–106.
- [54] X. He, S. Sanders, W.G. Aker, Y. Lin, J. Douglas, H.M. Hwang, Assessing the effects of surface-bound humic acid on the phototoxicity of anatase and rutile TiO₂ nanoparticles *in vitro*, *J. Environ. Sci.* (in press), doi: 10.1016/j.jes.2015.05.028.
- [55] S. McDonald, A.G. Bishop, P.D. Prenzler, K. Robards, Analytical chemistry of freshwater humic substances, *Anal. Chim. Acta* 527 (2004) 105–124.
- [56] C. Galindo, P. Jacques, A. Kalt, Photodegradation of the aminoazobenzene acid orange 52 by three advanced oxidation processes: UV/H₂O₂, UV/TiO₂

- and VIS/TiO₂: Comparative mechanistic and kinetic investigations, *J. Photochem. Photobiol., A: Chem.* 130 (2000) 35–47.
- [57] S. Kang, B. Xing, Humic acid fractionation upon sequential adsorption onto goethite, *Langmuir* 24 (2008) 2525–2531.
- [58] X. Ou, S. Chen, X. Quan, H. Zhao, Photochemical activity and characterization of the complex of humic acids with iron(III), *J. Geochem. Explor.* 102 (2009) 49–55.
- [59] S. Goldberg, H. Forster, C. Godfrey, Molybdenum adsorption on oxides, clay minerals, and soils, *Soil Sci. Soc. Am. J.* 60 (1996) 425–432.
- [60] M.U. Kumke, C.H. Specht, T. Brinkmann, F.H. Frimmel, Alkaline hydrolysis of humic substances—spectroscopic and chromatographic investigations, *Chemosphere* 45 (2001) 1023–1031.
- [61] J. Peuravuori, K. Pihlaja, Molecular size distribution and spectroscopic properties of aquatic humic substances, *Anal. Chim. Acta* 337 (1997) 133–149.
- [62] Y. Chen, N. Senesi, M. Schnitzer, Information Provided on Humic Substances by E4/E6 Ratios¹, *Soil Sci. Soc. Am. J.* 41 (1977) 352–358.
- [63] X. Guo, W. Du, X. Wang, Z. Yang, Degradation and structure change of humic acids corresponding to water decline in Zoige peatland, Qinghai-Tibet Plateau, *Sci. Total Environ.* 445–446 (2013) 231–236.
- [64] G. Liu, L. Liu, J. Song, J. Liang, Q. Luo, D. Wang, Visible light photocatalytic activity of TiO₂ nanoparticles hybridized by conjugated derivative of polybutadiene, *Superlattices Microstruct.* 69 (2014) 164–174.
- [65] K. Yang, B. Xing, Sorption of phenanthrene by humic acid-coated nanosized TiO₂ and ZnO, *Environ. Sci. Technol.* 43 (2009) 1845–1851.
- [66] L. Liang, L. Luo, S. Zhang, Adsorption and desorption of humic and fulvic acids on SiO₂ particles at nano- and micro-scales, *Colloids Surf., A: Physicochem. Eng. Aspects* 384 (2011) 126–130.
- [67] P. Persson, K. Axe, Adsorption of oxalate and malonate at the water-goethite interface: Molecular surface speciation from IR spectroscopy, *Geochim. Cosmochim. Acta* 69 (2005) 541–552.
- [68] B. Gu, H.E. Doner, The interaction of polysaccharides with silver hill illite, *Clays Clay Miner.* 40 (1992) 151–156.
- [69] B. Theng, Clay-polymer interactions: Summary and perspectives, *Clays Clay Miner.* 30 (1982) 1–10.
- [70] V.N.H. Nguyen, R. Amal, D. Beydoun, Effect of formate and methanol on photoreduction/removal of toxic cadmium ions using TiO₂ semiconductor as photocatalyst, *Chem. Eng. Sci.* 58 (2003) 4429–4439.
- [71] A.B. Giasuddin, S.R. Kanel, H. Choi, Adsorption of humic acid onto nanoscale zerovalent iron and its effect on arsenic removal, *Environ. Sci. Technol.* 41 (2007) 2022–2027.
- [72] Y. Cho, W. Choi, Visible light-induced reactions of humic acids on TiO₂, *J. Photochem. Photobiol. A: Chem.* 148 (2002) 129–135.
- [73] B. Gu, J. Schmitt, Z. Chen, L. Liang, J.F. McCarthy, Adsorption and desorption of natural organic matter on iron oxide: Mechanisms and models, *Environ. Sci. Technol.* 28 (1994) 38–46.
- [74] H. Baker, F. Khalili, A study of complexation thermodynamic of humic acid with cadmium (II) and zinc (II) by Schubert's ion-exchange method, *Anal. Chim. Acta* 542 (2005) 240–248.
- [75] H. Baker, F. Khalili, Comparative study of binding strengths and thermodynamic aspects of Cu(II) and Ni(II) with humic acid by Schubert's ion-exchange method, *Anal. Chim. Acta* 497 (2003) 235–248.
- [76] D. Lin, X. Tian, T. Li, Z. Zhang, X. He, B. Xing, Surface-bound humic acid increased Pb²⁺ sorption on carbon nanotubes, *Environ. Pollut.* 167 (2012) 138–147.
- [77] J. Buffle, W. Stumm, General chemistry of aquatic systems, *Chemical and Biological Regulation of Aquatic Systems*, vol. 1, CRC press, 1994, pp.1–42.
- [78] S.C. Myneni, T.I. Strathmann, Effect of soil fulvic acid on nickel (II) Sorption and bonding at the aqueous-boehmite (γ -AlOOH) interface, *Environ. Sci. Technol.* (2005) 4027–4034.